Multi-ionic effects on energy production based on double layer expansion by salinity exchange

M.M. Fernández, S. Ahualli, Guillermo R. Iglesias, Fernando González-Caballero, Ángel V. Delgado*, M.L. Jiménez

Department of Applied Physics, School of Sciences, University of Granada, 18071, Granada, Spain.

Abstract

It has been recently shown that the free energy change upon salinity mixing in river mouths can be harvested taking advantage of the fact that the capacitance of charged solid/liquid interfaces (electrical double layers, EDLs) depends strongly on the ionic composition of the liquid medium. This has led to a new generation of techniques called Capmix technologies, one of them (CDLE or Capacitive energy extraction based on DL Expansion) based precisely on such dependence. Despite the solution composition playing a crucial role on the whole process, most of the research carried out so far has mainly focused on pure sodium chloride solutions. However, the effect of other species usually present in river and sea waters should be considered both theoretically and experimentally in order to succeed in optimizing a future device. In this paper, we analyse solutions of a more realistic composition from two points of view. Firstly, we find both experimentally and theoretically that the presence of ions other than sodium and chloride, even at low concentrations, may lead to a lower energy extraction in the process. Secondly, we experimentally consider the possible effects of other materials usually dispersed in natural water (mineral particles, microbes, shells, pollutants) by checking their accumulation in the carbon films used, after being exposed for a long period to natural sea water during CDLE cycles.

Keywords: CapMix; Electric Double layer expansion; Energy extraction from salinity exchange; Ionic size effect; Multi-ionic solution.

1. Introduction

Since the original proposal of Pattle [1], a number of ideas have been envisaged in an attempt to obtain clean energy from salinity exchange when river and salty waters are mixed. Some of them are the results of investigations of the

*Corresponding Author

Email address: adelgado@ugr.es (Ángel V. Delgado)

physical chemistry of charged interfaces (electrical double layers, EDLs). This has originated the so-called Capmix techniques [2], a set of emergent technologies based on the direct capacitive extraction of energy starting from a salinity exchange. This family includes two groups of methods, one based on Donnan potential establishment in ion exchange membranes (CDP) [3–6], and the other associated to the EDL expansion when the ionic strength of the contacting solution is decreased (CDLE) [7–14]. Here we focus on the latter group, that is based on the lower capacitance of the EDL for more diluted solutions.

CDLE was firstly conceived by Brogioli [7], and implemented experimentally by Brogioli et al. [8]. The system consists of a couple of porous electrodes with high surface area (activated carbon, typically used in supercapacitors, is a good possibility) and assumed ideally polarizable, which are wet with sea water and charged at a voltage below 1 V to avoid the appearance of Faradaic reactions [15]. If salt water is exchanged by river water in open circuit (hence, constant charge conditions), a potential rise will take place, which allows discharging the electrodes at a potential higher than that used for charging. This is the origin of the positive energy balance.

Both theoretical models and experimental implementations of CDLE [10–14] are based on the simplest kind of exchanging solutions, namely, NaCl. All these efforts have led to the optimization of the characteristic parameters of the performance of the CDLE technique, but the description reached needs to be completed, as neither sea nor river waters are just NaCl solutions. Therefore, and in order to succeed in future implementations, the following two effects should be taken into account. Firstly, the use of natural ocean waters may have the drawback that materials (shells, sand particles, microbes) dispersed in water will affect the process by their deposition on the electrodes.

On the other hand, there is a wide variety of ions present in natural water. The effect of electrolyte mixtures with more than two ionic species have been investigated in many practical situations such as supercapacitor technology, water desalination, biological processes and electrokinetics [16–22]. In the case of CDLE, since this cycle directly depends on the electric double layer (EDL) structure, the electrolyte mixture can affect the extracted energy.

There have been several attempts to describe the structure of the EDL taking into account ionic size and valency by a generalization of the Poisson-Boltzmann equation [19, 23–27], (see also references in [26]). In these attempts, EDL overlap is usually neglected. However, inside 1 nm micropores, such approximation is not always fullfilled, even more so in the case of surface crowding associated to ions with finite volume [12, 28]. In this sense, Rica et al.[10] applied a modified Donnan model to the CDLE technique, in which a constant electric potential is assumed inside the micropores. However, this approximation is valid in the case of EDL thickness much larger than micropore size, which is not always the case.

In this paper, we analyze the significance of realistic solution composition for the CDLE technique. We first model and simulate it theoretically, taking into account both ionic size and valency, and possible EDL overlap. We apply such model to solutions of more than two ions, since the presence of finite concentra-

tions of Mg^{2+}, Ca^{2+}, SO_4^{-2} alters the charge-potential profiles, and, eventually, the energy production. We additionally perform experiments in which both natural and simulated water samples are used, paying special attention to the possible deposition of materials on the electrodes.

2. Theory

2.1. Principles of the technique

Fig. 1a is a schematic representation of the required setup. The porous electrodes are, in the first step, connected to a battery, a potentiostat, or a supercapacitor. Considering the highly porous nature of the carbon particles

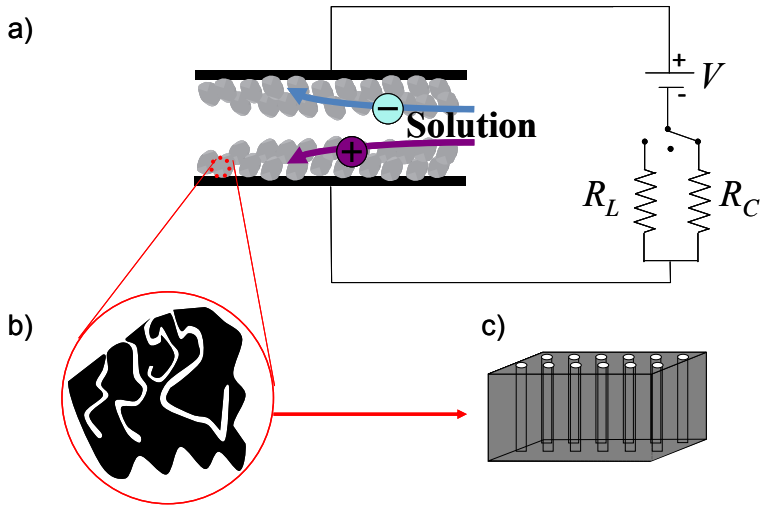

Figure 1: a) Schematic representation of the capacitive mixing cell; V is the charging voltage, R_C is the charging resistor, and R_L is the load resistor. b) Representation of a porous carbon particle. c) Swarm of cylinders simulating the pores.

(Fig. 1b), we have modelled them as an array of cylindrical pores, as shown schematically in Fig. 1c. Note that in reality the cylinders will be neither parallel not equally sized, but the present approach can be expected to properly catch the essentials of the EDL mechanisms of expansion. As to the existence of a distribution of pore diameters, the larger ones will act like channels providing the external salt concentration and present a much smaller surface area, so they will not be participating effectively in the process. Hence, we will include the following aspects in our simulations:

- Non-Planar EDL: inside the activated particles, the most abundant pores are typically less than 10 nm in diameter, and curvature effects on the electric potential profile can be significant.
- EDL overlap: it is likely in the smallest pores and with the less concentrated solutions, considering that the potentials used for charging can be relatively high.
- A charge-free region close to the interface (Stern layer) is assumed. Its size is determined by that of the ions.
- Ion-ion interactions will simply be considered under the excluded volume approximation.

Fig. 2 represents the energy extraction procedure [7]. The successive stages are as follows. A: electrodes in salt water connected to the battery at an initial potential Ψ_0 ($\Psi_0 = \pm V/2$, depending on the electrode considered); A→B: exchange for river water in open circuit (constant surface charge density σ_{AB} and subsequent potential rise to $\Psi_0 + \Delta\Psi_{fresh}$); B→C: battery reconnected in river water; C→D: exchange for salt water in open circuit (surface charge density σ_{CD} and voltage drop to $\Psi_0 - \Delta\Psi_{salt}$); D→A: battery reconnected in salt water. The area of the cycle represents the net extracted work per unit area of electrode. Hence, it is critical to properly calculate the relation between charge and potential at the EDL, in order to predict the experimental conditions leading to the maximum performance of the process. Parameters such as ionic size or charge affect such relation and they are the issue of this paper.

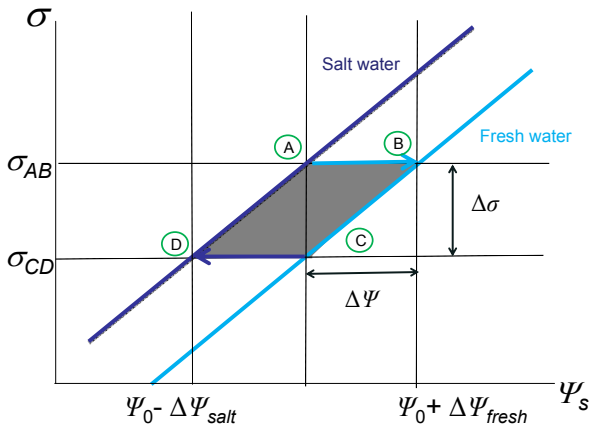

Figure 2: Schematic representation of the surface charge density vs. surface potential for two different concentrations. A possible CDLE cycle is marked by the gray shadowed region, and its area represents the energy extracted.

2.2. Theoretical model

We extend the model presented in [12] to multi-ionic solutions and cylindrical pores. Hence, we perform a mean field analysis of the structure of the EDL, and so, the electric potential distribution will be given by the Poisson equation:

$$\nabla^2\Psi(\mathbf{r}) = -\sum_{i=1}^{N} \frac{e\left(z_i c^i(\mathbf{r})\right)}{\varepsilon_m} \tag{1}$$

In this equation, Ψ is the electrostatic potential at position $\mathbf{r}$, e the electron charge, z_i and c^i are the valence and number concentration of the species i, N the number of the ionic species, and ε_m is the electric permittivity of the solvent. This equation will be solved subject to the following boundary conditions (r is the radial cylindrical coordinate with origin at the pore axis), specifying the surface potential of the pore wall, Ψ_S, and the zero electric field at the pore axis:

$$\Psi(r = R) = \Psi_S \tag{2}$$

$$\left.\frac{d\Psi}{dr}\right|_{r=0} = 0 \tag{3}$$

The relation between the ionic concentration and the electric potential at any point is based on the approximation provided in [19, 23, 24] which takes into account the excluded volume of ions:

$$c^i(\mathbf{r}) = \frac{c^i_\infty \exp\left[-\frac{z_i e\Psi(\mathbf{r})}{k_B T}\right]}{1 + \sum_i \frac{c^i_\infty}{c^i_{MAX}}\left[\exp\left(-\frac{z_i e\Psi(\mathbf{r})}{k_B T}\right)\right]} \tag{4}$$

where c^i_∞ and c^i_{MAX} denote, respectively, the bulk concentration and the maximum concentration allowed for the corresponding ionic species.

Note that we also take into account the excluded volume between particle surface and hydrated ions. This means that close to the surface there is a region inaccessible for ions, which is a zero-charge Stern layer. Hence, Eq. 1 must be solved separately in different regions. In the first one, between the particle surface and the radius of the smallest ion, say ion 1, $c^i(\mathbf{r}) = 0$. In the second region, where only the smallest ion can stay, we can write $c^{i\neq 1}(\mathbf{r}) = 0$. For the third region, where only ions 1 and 2 can stay, we can write $c^{i\neq 1,2}(\mathbf{r}) = 0$, and so on. Accordingly, new boundary conditions must be used, namely, the continuity of the potential and of the normal component of the electric displacement at the boundary between every pair of regions (we assume that the permittivity is the same in all regions):

$$\forall i = 1...N \begin{cases} \Psi(r = R - r_i^-) = \Psi(r = R - r_i^+) \\ \left.\frac{\mathrm{d}\Psi}{\mathrm{d}r}\right|_{r=R-r_i^-} = \left.\frac{\mathrm{d}\Psi}{\mathrm{d}r}\right|_{r=R-r_i^+} \end{cases} \tag{5}$$

Table 1: Salt concentrations used for simulated sea water [30]

Salt	Concentration (mmol/L)
NaCl	400
$MgSO_4$	20
$CaCl_2$ $2H_2O$	10
$MgCl_2$	20
KCl	10
Br	1.7

With these equations, the potential profile can be calculated as a function of the surface potential, the particle concentration, the pore size, and the ionic concentration. From the solution, we can obtain the surface charge density, σ, as [29]:

$$\sigma = -\varepsilon_m \frac{\mathrm{d}\Psi}{\mathrm{d}r}\Big|_{r=R} \tag{6}$$

Finally, the extracted work per unit interfacial area in every cycle is represented by the shadowed area in Fig. 2, which corresponds to:

$$W_S = \int_{\sigma_{CD}}^{\sigma_{AB}} \big[\Psi_S(C \to B) - \Psi_S(D \to A)\big]\mathrm{d}\sigma \tag{7}$$

Roughly speaking, the area is $\Delta\sigma\Delta\Psi$. This is important to be stated, because from this it is clear that the extracted work can be increased by increasing either the charge exchanged $\Delta\sigma$, the potential rise $\Delta\Psi$, or both.

3. Materials and Methods

As mentioned, both real (RSW) and simulated (SSW) sea waters were used in our experiments. Real samples were taken from the southern coast of Spain. In order to check for the possible negative effects of either organic or inorganic particulate material in real sea water, some experiments were also conducted after previously filtering the water through 16, 11 and 5 μm pore size. The water samples will be denominated 16RSW, 11RSW, and 5RSW, respectively. According to literature [30], SSW must contain the amounts of salts detailed in Table 1. In addition, as above described, 600 mM NaCl solutions will also be used as salty solution. The alternatives for river water simulation were 1/30 dilution of the corresponding salty solution.

The experimental CDLE data will be obtained using carbon layers deposited on a graphite film, as described in [6]. These carbon layers were made by mixing activated carbon powder with a binder solution. The powder was DLC Super 30, from Norit (The Netherlands), with a BET surface area of 1600 m^2/g. The solvent used (1-methyl 2-pyrrolidone, MP) was from Merck (Germany) and the binder, polyvinylidene fluoride (PVDF) was manufactured by Arkema (USA),

under the tradename Kynar HSV 900. All other chemicals employed were manufactured by Sigma-Aldrich (USA). The internal structure of the final carbon films was investigated by means of high-resolution scanning electron microscope observations, performed in a Gemini FESEM, from Carl Zeiss (Germany).

In Fig. 3a we show a picture of the measuring cell used. Two disks of the films (20 mm in diameter) were placed in the cell opposite to each other and separated by a 5 mm plastic spacer fixed in the middle of the cell. The disks were connected to the external circuit using platinum electrodes in contact with the graphite collectors. A microprocessor-controlled setup (PIC16F684, Microchip Technology Inc., USA) allows the control of the experiment while recording the data using a Keithley (USA) 2700 multimeter with a 7700 data acquisition card. The charging source was a Maxwell (USA) Bootscap 350 F supercapacitor connected to the cell through $R_C = 1\Omega$ resistor. In the discharge steps, the cell was also connected to this capacitor, through a $R_L = 20\Omega$ load resistor. Salty and river water reservoirs were placed some 50 cm above the electrode level, and two electrovalves were employed for filling the cell with the corresponding solution through the bottom tube.

Fig. 3b shows examples of successive CDLE cycles. We can identify the voltage increase when salty water is replaced by river water (A), the decrease when the external supercapacitor is reconnected (B), the further decrease when river water is replaced by salty water (C), and the final return to the initial state when the supercapacitor is connected again (D).

4. Results and Discussion

4.1. Theoretical predictions

The examination of the extracted work in the CDLE device with real solutions is complicated by the fact that the predominant ions apart from Na^+ and Cl^- differ from these in both size and valency. Both parameters will be examined separately before addressing the mixed solution.

4.1.1. Valency

In terms of a classical description of the EDL [29] it is easily demonstrated that increasing the valency implies a larger counterion concentration in the EDL for a given surface potential, and hence, a steeper reduction of the electric potential in it. As a consequence, the surface charge density for a given surface potential will be larger for multivalent counterions. This picture is modified if we take into account excluded volume effects between ions and also between ions and the surface. To clarify the effect of the valency in this case, we will consider in this section that all counterions have the same size (0.428 nm). In Fig. 4a,b we represent the electric potential and the volume charge density profiles inside the EDL for different counterion valencies and two coion concentrations ($c(Cl^-) = 0.02$ M and 0.6 M). For the pore radius examined ($R = 2$ nm) EDL overlap (non zero potential at the pore axis) is apparent, particularly for the less charged counterion. On the other hand, excluded volume effects produce a

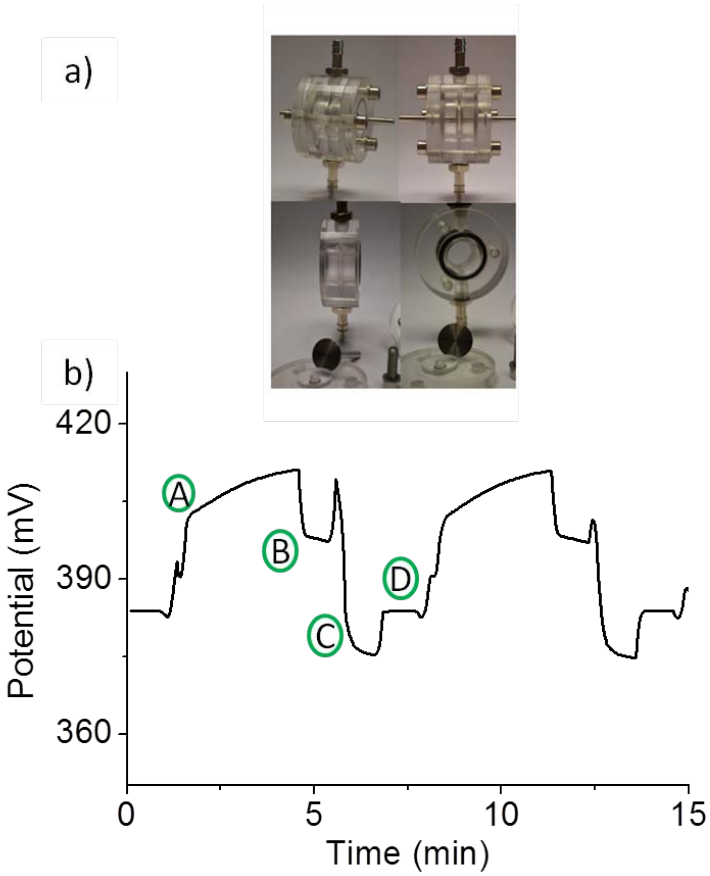

Figure 3: a) Picture of the cell used and its components. b) Voltage variation in successive experimental CDLE cycles.

maximum charge density (Fig. 4b) at the vicinity of the wall (this is magnified for the moderately high surface potential chosen, $\Psi_s = -500$ mV).

Fig. 4d shows the extracted work for different valencies of the ions in the solution. The presence of a maximum value at surface potentials below 0.3 V was already observed and discussed in [12]. This is an indirect consequence of the maximum attained by the EDL capacitance due to excluded volume effects between ions. Note that increasing the valency reduces the amount of extracted energy, and this can be explained by carefully examining Fig. 4c. There we can see that the expansion of the EDL due to dilution is less pronounced the larger the valency. As a consequence, while the stored charge is larger for higher valency as expected, the charge vs. surface potential curves corresponding to both salinities are closer in the latter case (Fig. 4c). This means that the voltage rise at constant charge ($\Delta\Psi$, Fig. 2) decreases and, as a consequence, the extracted work is also reduced (Fig. 4d).

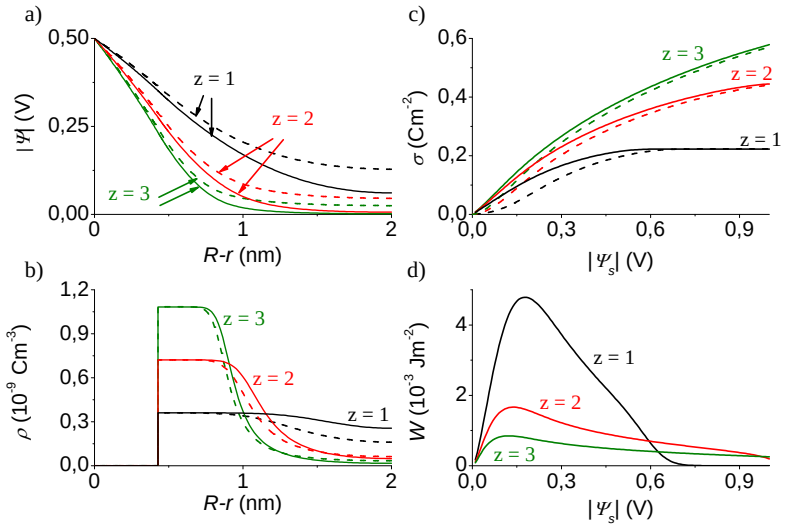

Figure 4: a) Electric potential and b) volume charge density profiles for a surface potential $\Psi_s = -500$ mV. Solid lines: c(Cl^-) = 0.6 M. Dashed lines: c(Cl^-) = 0.02 M. c) Surface charge density vs. surface potential for the same ionic strengths. d) Extracted work per unit area of pore when the solutions considered in a), b), c) are exchanged. In all cases, the valency of the cation is indicated. Ion size: 0.428 nm. Pore radius: 2 nm.

4.1.2. Effect of ionic size

The profiles of electric potential and volume charge density in the EDL are plotted in Fig. 5a and b for different ionic sizes and different surface potentials. The region of charge density saturation close to the pore wall extends over longer distances the larger the ionic size. The larger ionic volume in this case produces as well a lower value of the saturation charge density, a larger empty Stern layer, and a slower potential decay in the EDL. As a consequence, the surface charge density decreases by increasing the size of the ions, as can be seen in Fig. 5c.

The consequences of this EDL structure on the amount of extracted work are illustrated in Fig. 5d. We can see that increasing the ionic size leads to a decrease of the maximum energy that can be extracted per unit area in every CDLE cycle, mostly because increasing the ionic size produces a decrease of $\Delta\sigma$ of the cycle. This can be compared to the valency effect (Fig. 4d) mainly associated to a reduction of $\Delta\Psi$ upon exchanging salinity in the CDLE cycle.

4.1.3. Multi-ionic solutions

From the above results, we can expect a lower energy production when the counterion is Mg^{2+} (valency 2, ionic size 0.428 nm) as compared to Na^+ (valency 1, ionic size 0.358 nm). However, we will find below that new aspects must be taken into account when several counterions with different valencies and sizes compete for the volume close to the surface. Furthermore, the concentration of Na^+ and Cl^- in natural water is far larger than that of other bigger and more

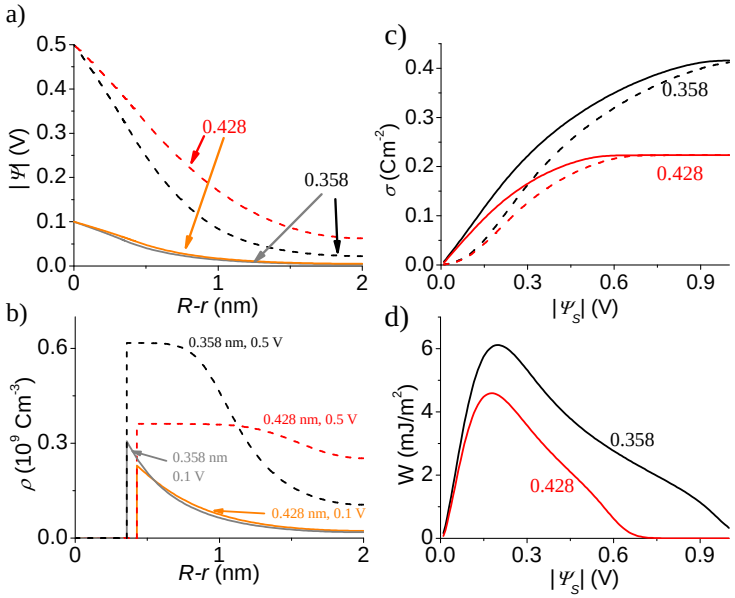

Figure 5: a) Electric potential and b) volume charge density profiles for surface potentials 0.5 V and 0.1 V, and salt concentration 600 mM. c) Surface charge density vs. surface potential for an ionic concentration 600 mM (solid lines) and 20 mM (dashed lines). d) Extracted work as a function of the surface potential upon exchanging the solutions in c). In all cases the cation valency is $z = 1$. The cation radii in nm are indicated. Pore size: 2 nm.

charged species. For simplicity we present the simplest case: two counterions and one coion. We choose Na^+ and Mg^{2+} and the concentrations are given in order to preserve both their ratio in the sea and electroneutrality with respect to the coion (Cl^-) concentration. These values are listed in Table 2A.

The different volumes of Na^+ and Mg^{2+} are accounted for in our model by considering that the maximum concentration attained by Mg^{2+} ions is smaller and the distance of closest approach to the surface is larger than in the case of Na^+ ions. Information about the structure of the EDL in this case is presented in Fig. 6. We observe that close to the particle there is an empty region followed by a region in which only Na^+ can be present. When we depart a distance sufficient to allow the presence of Mg^{2+}, the concentration of Na^+ decreases, because the volume is occupied by the more charged Mg^{2+} ions. The effect is magnified for large surface potential (Fig. 6b). In this case, Na^+ concentration decays to zero as a consequence of the Mg^{2+} condensation close to the wall.

Hence, for moderate to large potentials, and despite the small concentration of Mg^{2+} as compared to that of Na^+, as soon as it saturates the interface, it determines the extracted work (Fig. 6c), since it is larger than Na^+ and gives rise to a lower stored charge. Because of its higher valency, the EDL expansion is also lower, and as a result, the extracted work is reduced.

Table 2: Ionic concentrations selected for simulations of sea and river waters [31]

A: 3 ions		
Ion	River Concentration (mol/L)	Sea Concentration (mol/L)
Cl^-	0.02	0.6
Na^+	0.0167	0.5
Mg^{2+}	0.00167	0.05
B: 4 ions		
Cl^-	0.019	0.57
SO_4^{2-}	0.0005	0.015
Na^+	0.0167	0.5
Mg^{2+}	0.00167	0.05

For the sake of clarity, in Fig. 6c we compare the results with those obtained when only one counterion is present, but in the concentration that it would actually have in the river or sea waters. These concentrations simulate the case of an hypothetical previous cleaning of the water from one of the cations. We can see that the extracted work in Fig. 6c is not the sum of the works extracted from "clean" waters containing only Mg^{2+} or Na^+, but an intermediate value, which is determined by the fact that Na steps aside when Mg is present and hence, determines the expansion of the EDL. Note also that the effect is very large, in spite of the small amounts of the bigger ions.

Let us finally consider the whole picture with the most abundant ions in the sea: Cl^-, SO_4^{2-}, Na^+, Mg^{2+} and take into account that the CDLE device consists of two oppositely charged electrodes, not symmetric because of the different sizes and concentrations of their counterions. In a real cycle, charge will be transferred from the positive electrode to the negative one, and hence, the measured potential rise would be the difference between those in each electrode: $V = \Psi_S^+ - \Psi_S^- = \Psi_S^+ + |\Psi_S^-|$. In Fig. 7a it is represented the surface charge density vs. surface potential between the electrodes for two cases: only Na^+ and Cl^- and the four ions mentioned. Again, although the mixture provides larger surface charge, the curves corresponding to 20 mM and 600 mM approach each other and hence, the CDLE cycle narrows. The effect on the extracted work is presented in Fig. 7b as a function of the potential difference between the electrodes. It is again confirmed that removing large multivalent ions from the solution will give out larger extracted work.

4.2. Experimental results

When natural water is used as fuel for a CDLE cycle, there are two aspects to take into account when results are eventually compared to laboratory-prepared NaCl solutions. On one hand, energy production can be altered by the mere change in composition, as we have shown above that both valency and size of counterions can substantially modify the EDL structure and hence the cycle area. On the other hand, natural waters contain suspended material which can additionally produce long-time effects such as electrode corrosion, fouling, etc.,

which must be properly addressed. This will be dealt with in the following paragraphs.

4.2.1. Study of electrode contamination

Prior to the comparison between NaCl and multi-ionic solutions, it appears interesting to analyze, from an experimental point of view, the effect of substances other than ionic species. For this purpose, we have used real sea water in a CDLE cycle, analyzing the effect of the deposits on the electrodes. With that aim, we performed a systematic scanning electron microscope evaluation of the carbon film, considering both transversal cuts of the carbon films, and also a top view of it. An EDX analysis was carried out on specific sites of the samples, in order to ascertain the possible presence of such impurities.

Fig. 8 shows a transversal view of the carbon film. We can observe the graphite collector which is just below the carbon porous plug. The material composition is mainly carbon as it is shown in EDX analysis in Fig. 8. Note that a very small amount of materials from the sea water can go all the way through the carbon film. As expected, these are mainly silica or silicates and NaCl. The situation is, as expected, less pristine on the top of the film, that is, the area in immediate contact with the solutions. Fig. 9 shows the presence of considerable amounts of Si in some spots (deposited sand particles), and, interestingly, iron. This can come from oxides also in suspension or from corrosion from the valves used.

Although SEM pictures show that some impurities are however observable, both inside the carbon plug and, specially on top of it, it is surprising to find out that we rarely observe an important deposition on the carbon films after being exposed to natural sea water. Hence this drawback may not be crucial. This may be due to the large amount of river water that is used during the exchange process.

Some idea can be gained from the analysis of the materials deposited on the filters (Fig. 10) after natural sea water purification: EDX analysis (not shown) of areas of the pictures demonstrate the presence of spherical particles containing iron (probably iron oxide), as well as silica or silicates and calcium from shells of small animals.

These observations may explain that the negative effect of natural sea water deposits on the cycle performance, although certainly existent, is lower than expected at first sight: Fig. 11 shows that only when the filtration is brought to the low practical limit of 5 μm can we say that the value corresponding to artificial sea water is recovered, and water can be considered sufficiently free of impurities from the viewpoint of the CDLE technique. This could be expected from the SEM pictures in Figs. 8 and 9. There is no important deposition on the carbon film that would lead to a reduction of the extracted energy.

4.2.2. Influence of solution composition

In order to analyze the effect of the multi-ionic composition of natural water, we study separately the branches of the cycle where sea and river waters are in contact with the electrodes and with river water. Hence, we firstly fixed river

Table 3: Comparison of the voltage rise, extracted charge, and energy per cycle obtained with 20 mM NaCl and RSW diluted 30 times as river water, in otherwise identical conditions: charging voltage $\approx$ 380 mV. 16 RSW is used as salt water fuel

River Water	Potential rise (mV)	Extracted charge (mC)	Energy (μJ)
20mM	20.60 $\pm$ 0.17	1.64 $\pm$ 0.08	18 $\pm$ 1
1/30 RSW	13.6 $\pm$ 0.6	1.09 $\pm$ 0.04	7.8 $\pm$ 0.6

water at 20 mM NaCl concentration and studied the effect of using either NaCl 600 mM, SSW or RSW. Fig. 12 shows the behavior of the CDLE cycles in the three cases. In Fig. 12a some examples are shown of the voltage variation when successive cycles are performed in the three cases. In this plot, the decrease of the voltage rise when either simulated or real sea waters are used is qualitatively demonstrated. A quantitative view is provided in Fig. 12b, where it can be observed that both the potential rise upon salinity exchange and the transferred charge upon battery reconnection are reduced when simulated or real sea waters are used. As a consequence, the extracted energy is greatly reduced (Fig. 12c). This is in agreement with our theoretical predictions: despite the increase in the valency, the presence of multi-ionic solutions reduces the cycle performance, by reducing the charge transferred and the voltage rise. The effect is most important when RSW is used.

Not only the overall result of a complete CDLE cycle is affected. The dynamics of the surface voltage upon exchanging salty and river waters may also be affected, since the diffusion coefficients are larger for Na^+ and Cl^- (respectively, 1.33×10^{-9} and 10^{-9} m^2/s) than for Mg^{2+} (0.70×10^{-9} m^2/s) and SO_4^{2-} (1.06×10^{-9} m^2/s). Indeed, this can be observed with a detailed analysis of the dynamics of the voltage after exchanging the solution, especially upon the river water exchange as it is presented in Fig. 13. There, it is confirmed that the rate of voltage variation is also dependent on the kind of salt, and in fact the rise appears slower for the sea waters (either simulated or natural) than for NaCl solutions.

Next, we maintain the same sea water (in this case we use a filtered sample, 16RSW) and we measure the voltage rise for two different kinds of river water. A standard real river water is difficult to set, since the variability in river water composition is even larger than in sea water: it depends on the river basin, and even for the same river basin, it changes with the season, the rain regime, the human activities upstream, and so on. But it is evident that the performance of the CDLE cycle will be seriously compromised if the salt contents of the river is excessive and it can be expected that the analysis in this case can shed some light on the real possibilities of this technique. The results of using a simulated river water as 1/30 dilution of the sea water are shown in Table 3. The decrease in both the voltage rise upon salinity exchange and the transferred charge upon supercapacitor reconnection produces a reduction of the energy extracted in comparison to that obtained when pure NaCl solutions are used.

5. Conclusions

Capacitive energy production based on double layer expansion (CDLE) is a promising technology through which exchanging two solutions of different salinity in contact with conducting electrodes a net amount of clean, renewable net energy can be obtained. In this paper we present a study of the effect of using realistic water compositions in CDLE cycles. We have experimentally observed that the main difference in the extracted energy (as compared to NaCl solutions) comes from the presence of multivalent ions, due to the fact that other species rarely produce deposits on the electrodes, as we have demonstrated with electron microscope observations. Despite the small amount of multivalent ions in sea and river waters, they contribute with a measurable decrease in the extracted energy. We have presented a model capable of predicting such behavior: multivalent ions produce a decrease of the double layer expansion responsible for the net energy gain in a CDLE cycle. Also, the larger size of these ionic species is responsible for the decrease of the stored charge at the electrodes. These two factors working together bring about a reduction of the extracted energy in spite of the small relative concentrations of the larger, divalent ions. Continuation of this study should, first of all, include a theoretical treatment of the kinetics of the CDLE process using different water compositions. Experimental investigation should focus on the possible advantage of pretreating the sea water in order to minimize the amount of multivalent ions present, and the final step will involve working on site in different locations and during long periods. The evolution of the energy obtained and the consistency of the electrodes will give clues as to the true effect of employing natural waters in CDLE. Ideally these tests should be carried out in parallel with other techniques based on salinity gradient energy, such as PRO and RED.

Acknowledgements

The research leading to these results received funding from the European Union 7th Framework Programme (FP7/2007-2013) under agreement No. 256868. Financial support from Junta de Andalucia (Project PE2012-FQM 694) and MINECO (Project FIS2013-4766-C3-1-R) is also acknowledged. One of us, M.M.F., is grateful to the University of Granada for her FPU grant.

References

[1] R. E. Pattle, Nature 174 (1954) 660–660.

[2] M. Bijmans, O. Burheim, M. Bryjak, A. Delgado, P. Hack, F. Mantegazza, S. Tenisson, H. Hamelers, Energy Procedia 20 (2012) 108 – 115.

[3] B. B. Sales, M. Saakes, J. W. Post, C. J. N. Buisman, P. M. Biesheuvel, H. V. M. Hamelers, Environ. Sci. Technol. 44 (2010) 5661–5665.

[4] B. B. Sales, F. Liu, O. Schaetzle, C. J. Buisman, H. V. Hamelers, Electrochim. Acta 86 (2012) 298 – 304.

[5] O. S. Burheim, F. Liu, B. B. Sales, O. Schaetzle, C. J. N. Buisman, H. V. M. Hamelers, J. Phys. Chem. C 116 (2012) 19203–19210.

[6] F. Liu, O. Schaetzle, B. B. Sales, M. Saakes, C. J. N. Buisman, H. V. M. Hamelers, Energy Environ. Sci. 5 (2012) 8642–8650.

[7] D. Brogioli, Phys. Rev. Lett. 103 (2009) 058501.

[8] D. Brogioli, R. Zhao, P. M. Biesheuvel, Energy Environ. Sci. 4 (2011) 772–777.

[9] D. Brogioli, R. Ziano, R. A. Rica, D. Salerno, O. Kozynchenko, H. V. M. Hamelers, F. Mantegazza, Energy Environ. Sci. 5 (2012) 9870–9880.

[10] R. A. Rica, D. Brogioli, R. Ziano, D. Salerno, F. Mantegazza, J. Phys. Chem. C 116 (2012) 16934–16938.

[11] R. A. Rica, R. Ziano, D. Salerno, F. Mantegazza, D. Brogioli, Phys. Rev. Lett. 109 (2012) 156103.

[12] M. Jiménez, M. Fernández, S. Ahualli, G. Iglesias, A. Delgado, J. Colloid Interface Sci. 402 (2013) 340 – 349.

[13] R. A. Rica, R. Ziano, D. Salerno, F. Mantegazza, M. Z. Bazant, D. Brogioli, Electrochim. Acta 92 (2013) 304 – 314.

[14] G. R. Iglesias, M. M. Fernández, S. Ahualli, M. L. Jiménez, O. P. Kozynchenko, A. V. Delgado, J Power Sources 261 (2014) 371–377.

[15] B. Conway, Electrochemical Supercapacitors: Scientific Fundamentals and Technological Applications, Kluwer Academic, New York, 1999.

[16] R. Lin, P.-L. Taberna, S. Fantini, V. Presser, C. R. Prez, F. Malbosc, N. L. Rupesinghe, K. B. K. Teo, Y. Gogotsi, P. Simon, The Journal of Physical Chemistry Letters 2 (2011) 2396–2401.

[17] R. Palm, H. Kurig, K. Tnurist, A. Jnes, E. Lust, Electrochemistry Communications 22 (2012) 203 – 206.

[18] P. Biesheuvel, Y. Fu, M. Bazant, Russ. J. Electrochem. 48 (2012) 580–592.

[19] J. J. López-García, M. J. Aranda-Rascón, C. Grosse, J. Horno, J. Phys. Chem. B 114 (2010) 7548–7556.

[20] T.-L. Horng, T.-C. Lin, C. Liu, B. Eisenberg, The Journal of Physical Chemistry B 116 (2012) 11422–11441.

[21] B. Lu, Y. Zhou, Biophysical Journal 100 (2011) 2475 – 2485.

[22] S. Ahualli, M. M. Fernández, G. Iglesias, M. L. Jiménez, F. Liu, M. Wagterveld, A. V. Delgado, J. Phys. Chem. C (2014) –. doi:http://dx.doi.org/10.1021/jp504461m.

[23] Z. Adamczyk, P. Warszynski, Adv. Colloid Interface Sci. 63 (1996) 41–149.

[24] I. Borukhov, J. Polymer Sci. Part B-Polymer Phys. 42 (2004) 3598–3615.

[25] M. Z. Bazant, M. S. Kilic, B. D. Storey, A. Ajdari, Adv. Colloid Interface Sci. 152 (2009) 48–88.

[26] H. Wang, A. Thiele, L. Pilon, The Journal of Physical Chemistry C 117 (2013) 18286–18297.

[27] A. Yochelis, The Journal of Physical Chemistry C 118 (2014) 5716–5724.

[28] M. Z. Bazant, B. D. Storey, A. A. Kornyshev, Phys. Rev. Lett. 106 (2011) 046102.

[29] J. Lyklema, Fundamentals of Interface and Colloid Science, vol. II: Solid-Liquid Interfaces, Academic Press, New York, 1995.

[30] J. Mclachlan, Can. J. Microbiol. 10 (1964) 769–782.

[31] D. R. Kester, I. W. Duedall, D. N. Connors, R. M. Pytkowicz, Limnology & Oceanography 12 (1967) 176–179.

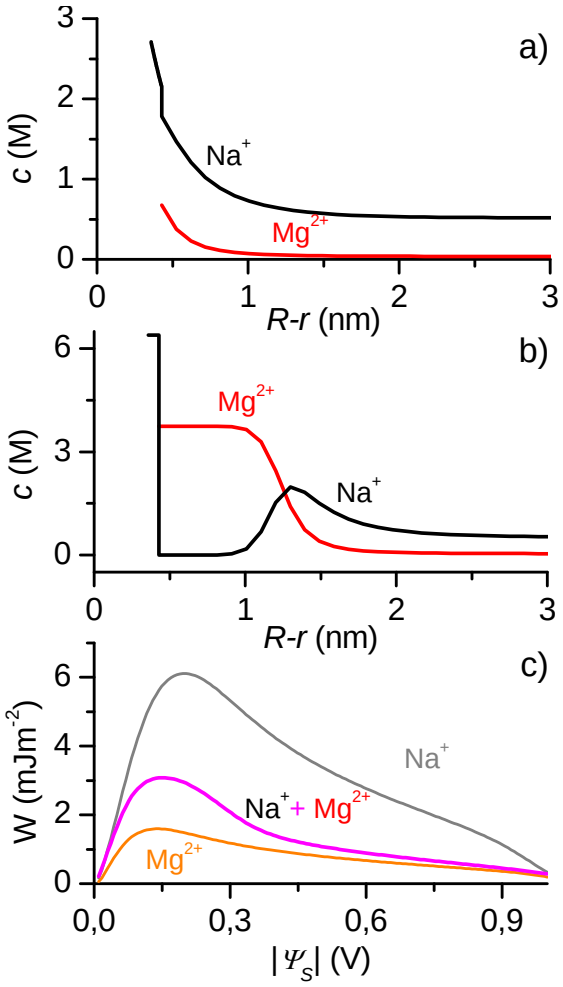

Figure 6: Counterion concentration profiles for the sea composition given in Table 2A and surface potentials 0.1 V (a) and 1 V (b). c) Extracted work per unit area vs. surface potential in the following cases: only Na^+ (sea concentration: 600 mM, river concentration: 20 mM); only Mg^{2+} (respective concentrations: 300 mM and 10 mM); both counterions present, with concentrations as in Table 2A. Pore radius 10 nm.

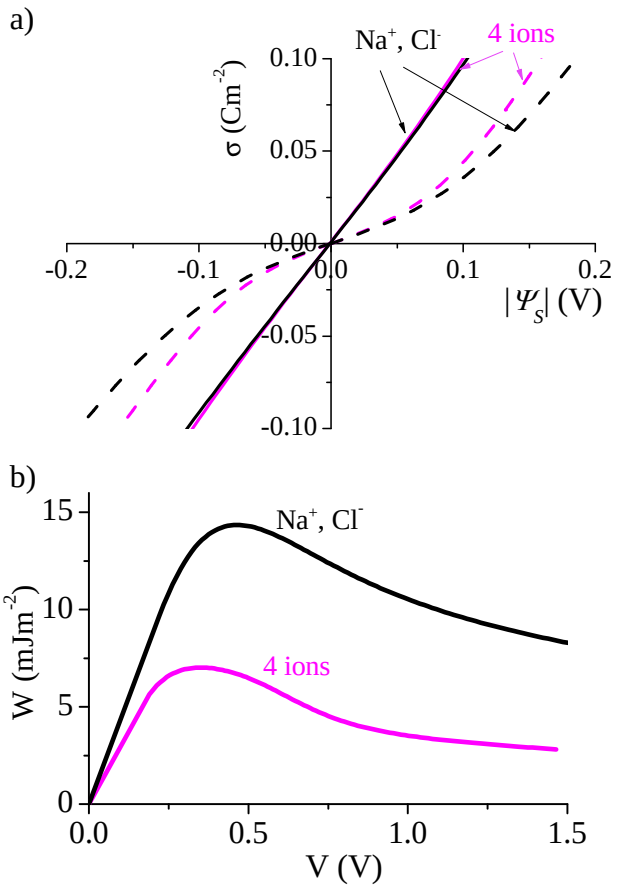

Figure 7: a) Surface charge vs. surface potential for 20 mM (dashed lines) and 600 mM (solid lines). b) Extracted work per unit area vs. the potential of the external battery. "4 ions" indicates that all ions in Table 2B are present with the concentrations there indicated. Pore radius 10 nm.

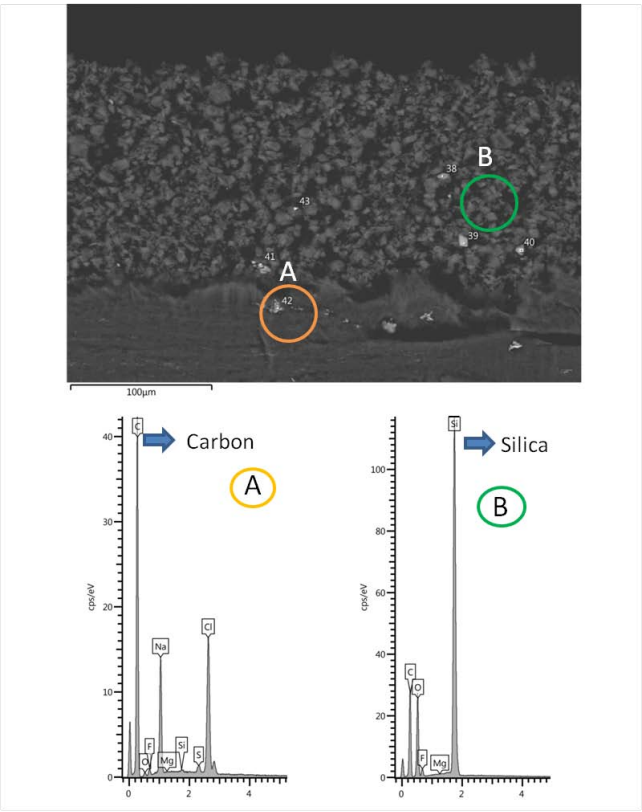

Figure 8: Top: SEM picture of the section of the carbon film after cycling natural sea water and 20 mM NaCl solution. Bottom: EDX spectra of the areas marked as A and B of the picture.

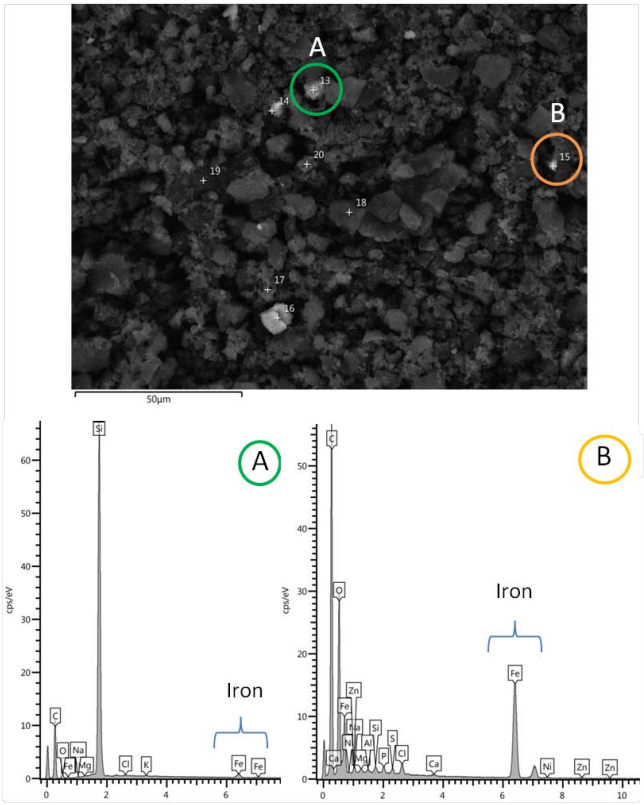

Figure 9: Top: SEM picture of the top of the carbon film after cycling natural sea water and 20 mM solution. Bottom: EDX spectra of the areas marked as A and B of the picture.

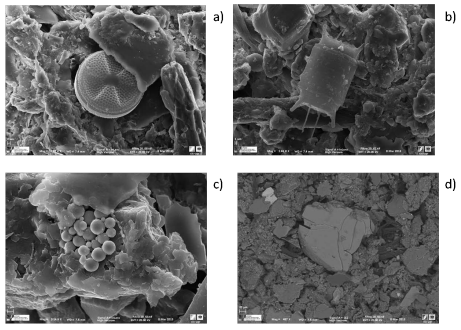

Figure 10: SEM pictures of the 16 μm filters after filtering natural sea water. (a,b) detail of deposited organic shells; (c,d): inorganic impurities.

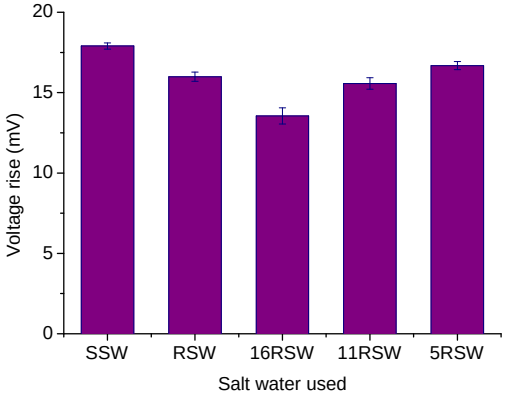

Figure 11: Voltage rise in the sea-to-river water step when diluted RSW is used as river water against RSW, with and without previous filtering through 5, 11 and 16 μm filter pore size.

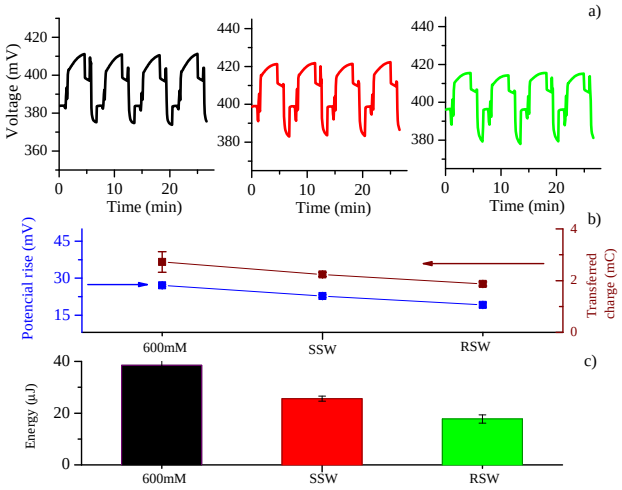

Figure 12: a) Examples of successive CDLE cycles when NaCl 600 mM (left), simulated sea water (center) and real sea water (right) are used. b) Potential rise (blue, left axis) and transferred charge (dark red, right axis) for the three salty waters examined. c) Extracted energy. In all cases, the river water is simulated with 20 mM NaCl solutions.

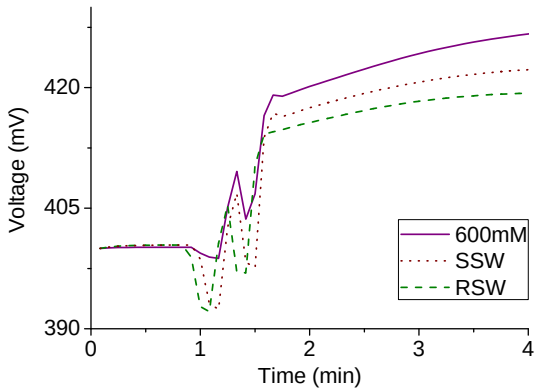

Figure 13: Detail of the sea-to-river water exchange part of the CDLE cycle, after shifting vertically the data in Fig. 12 for making the starting voltages coincident.